80-Myr history of buoyancy and volcanic fluxes along the trails of the Walvis and St. Helena hotspots (South Atlantic)

Claudia Adam [a,*], Valerie Vidal [b], Javier Escartín [c]

[a] *Institute for Research on Earth Evolution, Japan Agency for Marine-Earth Science and Technology, 2-15 Natsushima, Yokosuka, 237-0061, Japan*
[b] *Laboratoire de Physique, Ecole Normale Supérieure de Lyon-CNRS, 46 Allée d'Italie, 69364 Lyon cedex 07, France*
[c] *Laboratoire de Géociences Marines- CNRS, Institut de Physique du Globe de Paris, case 89, 4 place Jussieu, 75252 Paris cedex 05, France*

Abstract

Walvis and St. Helena are the only long-lived hotspot chains in the South Atlantic. Therefore, their characterization is important to constrain the processes associated with mantle plume formation, their temporal evolution, and the interaction with plate and mantle dynamics in the region. We study the temporal evolution of plume buoyancy and magma production rate along both hotspot chains, which are constrained from the swell and volume of volcanic materials emplaced along the chain. The regional depth anomaly is calculated by correcting the 2′ bathymetry grid of Smith and Sandwell [W.H.F. Smith, D.T. Sandwell, Global sea floor topography from satellite altimetry and ship depth soundings, Science 277 (1997) 1956–1962] for thermal subsidence and sediment loading. We separate the topography associated with volcanism and the swell surrounding the hotspot chains using the MiFil filtering method [C. Adam, V. Vidal, A. Bonneville, MiFil: A method to characterize seafloor swells with application to the south central Pacific, Geochem. Geophys. Geosyst. 6 (1) (2005) Q01003, doi: 10.1029/2004GC000814]. We then estimate the temporal variations associated with both parameters by computing volumes along the hotspot tracks. Neither Walvis nor St. Helena show a 'classical' hotspot behavior. We find that two plumes are at the origin of the St. Helena chain. This study also shows a swell associated with the Circe seamount, supporting the existence of a hotspot NW of the St. Helena trail. The variation in swell and volcanic fluxes suggests temporal variability in the plume behavior at time scales of 10–20 m.y. and 5 m.y., which may be related to oscillations and instabilities of the plume conduit, respectively. Cumulative fluxes in the area are largest for Walvis and weakest for Circe, and all are significantly lower than that reported for the Hawai'i hotspot.
© 2007 Elsevier B.V. All rights reserved.

1. Introduction

Hotspot chains are the result of the interaction of stationary zones of mantle upwelling (plumes) with an overlying drifting plate (Wilson, 1963). Two main surface manifestations are generally associated with such a plume–lithosphere interaction: (1) a prominent

* Corresponding author.
   E-mail addresses: adam@jamstec.go.jp (C. Adam),
Valerie.Vidal@ens-lyon.fr (V. Vidal), escartin@ipgp.jussieu.fr
(J. Escartín).

volcanic chain which displays a linear age progression, as plate motion drags the seamounts away from their zone of emplacement above the plume; and (2) a large positive depth anomaly (typically 100's of kilometers in extent and ~100's of meters in height) called a swell (Crough, 1983). The hotspot swells may be produced by several phenomena. Dynamic topography, associated with vertical forces due to plume uplift, may generate a swell (a few hundred meters in height) in the youngest part of the hotspot chain, where the lithosphere drifts over the plume head. The swell at older parts of the hotspot chain may have two origins: 1) A thinner than 'normal' lithosphere, due to reheating at the time the lithosphere was overriding the hotspot plume. This effect vanishes through time, as the lithosphere cools and subsides while it is driven away from the plume. 2) Stocking of plume material within or beneath the lithosphere or crust (underplating), which has a permanent effect. Since no underplating has been identified along St. Helena and Walvis chains, and since the dynamic topography is spatially restricted along the youngest part of these chains, we attribute the main cause of the swell to the long-term thermal effect of the plume.

The swell is a direct consequence of the buoyant plume upwelling, and therefore, it is commonly used as the parameter to quantify the hotspot strength (Sleep, 1990; Courtillot et al., 2003; Vidal and Bonneville, 2004). However, this parameter is inadequate to study the history of a hotspot chain and the underlying plume dynamics, as the swell amplitude decreases with time due to lithospheric cooling. The volcanic material accumulated along the hotspot chain, which is not affected by this cooling, is a direct record of the volcanic output to the seafloor. However, while being a good indicator of hotspot activity, the volume of extrusives may somewhat underestimate the total melt production, as other processes may operate such as melt entrapment in deep lithospheric levels, or lateral melt migration (i.e., lithospheric cracks) and emplacement away from the volcanic chain. The combined analyses of both swell and volcanic volumes accumulated along the chain is therefore most adequate and necessary to constrain long-term plume activity (Vidal and Bonneville, 2004).

In this study, we use the available bathymetric (Smith and Sandwell, 1997), sediment thickness and seafloor age data (Müller et al., 1997) to correct for thermal subsidence and sediment loading, and obtain a seafloor depth anomaly around the Walvis and St. Helena hotspot chains. We then separate the swell and volcanic topography components from the residual bathymetry (Adam et al., 2005). We then estimate the temporal evolution in production rate of volcanic material Q_v (including both the volcanic edifices and compensating root due to plate flexure) and in the swell flux Q_s. We compare these results with those from Hawai'i (Vidal and Bonneville, 2004), the most typical example of a hotspot chain.

2. Tectonic setting

2.1. Description of the Walvis and St. Helena chains

Walvis and St. Helena are the two main hotspot chains found in the South Atlantic. They are formed by wide and continuous zones of diffuse volcanism (oceanic islands, seamounts and small ridges), that locally reach a width of more than 500 km. It is generally considered that these volcanic chains have been created by mantle plumes interacting with the overlying African plate, and that the locus of present-day activity is situated in the proximity of the Island of Tristan da Cunha for the Walvis Ridge. For St. Helena, the youngest age of volcanism (2.6 Ma) is reported at Josephine seamount (O'Connor et al., 1999; Courtillot et al., 2003) (see Fig. 1). This is consistent with the reported general age progression of volcanism away from the St. Helena and Gough islands and towards the African continent (O'Connor and Duncan, 1990; O'Connor and le Roex, 1992).

The Walvis Ridge extends WSW some 2800 km from the southwest African continental margin towards the Mid-Atlantic Ridge near Tristan da Cunha and Gough islands (Fig. 1). Based on morphological and structural characteristics, the chain displays different tectonic settings at the time of volcanic emplacement and loading. The northeastern part (east of 3°E) has a ridge-like, elongated morphology rising 2–3 km above the surrounding seafloor. Large-scale block faulting in this area is prominent, as inferred from the gravity, bathymetry and seismic data (Goslin and Sibuet, 1975; Detrick and Watts, 1979). Further southwest, the ridge splits into two branches, one trending N–S and a second one trending NE–SW, both composed of individual seamounts and guyots. The N–S trending branch terminates near 34°S, whereas the oblique branch continues WSW towards the present-day hotspot location on the eastern flank of the Mid-Atlantic Ridge. The initial manifestation of the Walvis hotspot occurred at the opening of the South Atlantic 130 Ma ago, when it contributed to the emplacement of the Paraná (Southeast Brazil) and Etendeka (southwest Africa) flood basalts, 127.5 to 139 Ma old (Gibson et al., 2006). The hotspot was located initially on the American plate, crossed the
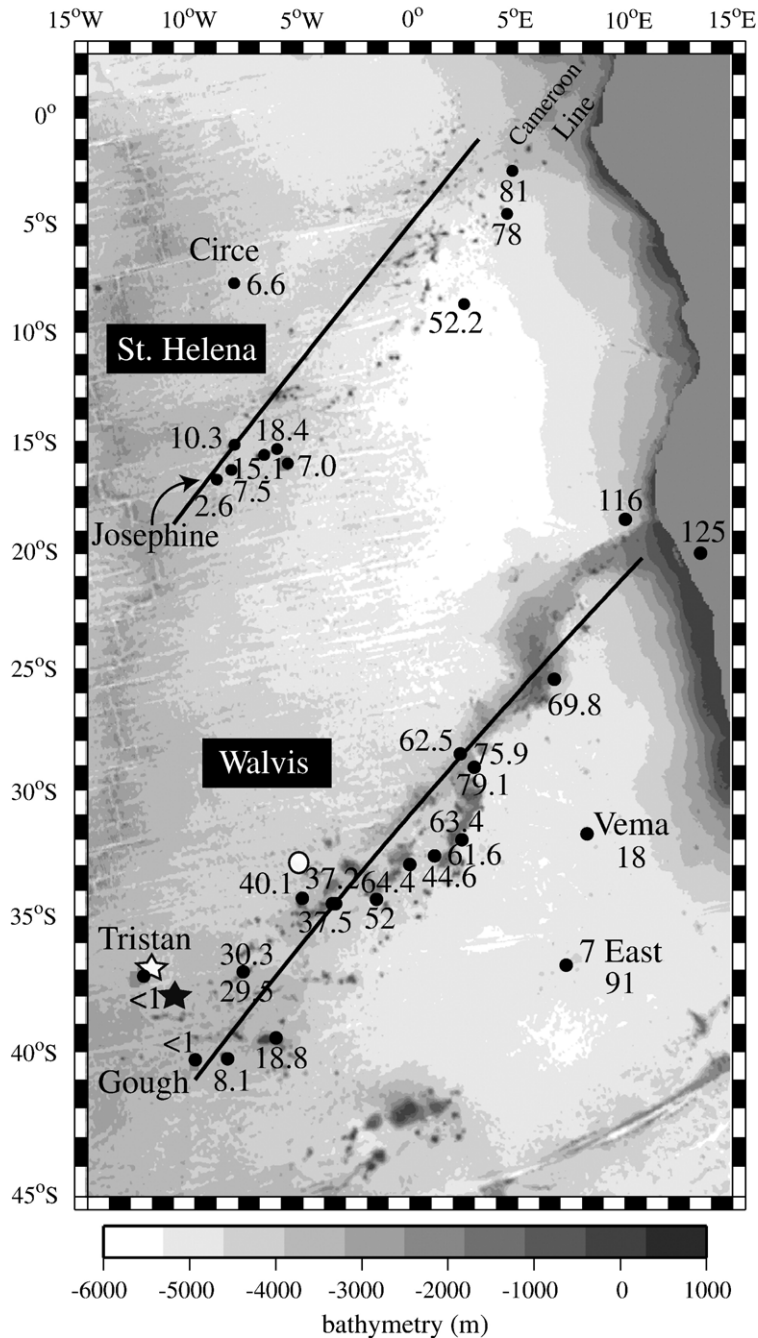
Fig. 1. Bathymetry of St. Helena and Walvis chains (2′ bathymetry grid from Smith and Sandwell, 1997), and published volcanic ages (in million years, from O'Connor and Duncan, 1990; O'Connor and le Roex, 1992). Black lines indicate the traces used to study the temporal evolution of hotspot fluxes (see text for discussion). The white and black stars indicate the present-day location of the Walvis plume inferred by Courtillot et al. (2003) and Steinberger (2000), respectively. The white dot on Walvis northern edge indicates the location of presumed present-day underwater volcanism as inferred from hydrophone events (Haxel and Dziak, 2005).

axis 80–70 Ma ago, and progressively separated from it to its present-day location on 7 Ma-old African plate.

Evidence for this transition from on-axis to intraplate volcanism is found in many geophysical and geochem-

ical observables. The geochemical analyses evidence a westward migration of the spreading axis, away from the plume (O'Connor and Duncan, 1990; Schilling et al., 1985). The structural differences between the

northeast (oldest) and southwest (youngest) sections of the chain are also reflected in their compensation mechanisms. While the older part is compensated by over-thickening of the oceanic crust (Goslin and Sibuet, 1975; Detrick and Watts, 1979), the western part is instead regionally compensated by the bending of a lithosphere with an effective elastic thickness of 5−8 km (Detrick and Watts, 1979). These different compensation mechanisms reflect the transition with time from a near-axis emplacement with a thin lithosphere and over-thickened crust to an intraplate setting with a thicker lithosphere. This transition is also observed in the mode of volcanic emplacement, that produces at first a structurally continuous ridge, and then a province of intermittent, isolated volcanoes.

The St. Helena chain is less defined, and is characterized by a broad and ill-defined band of scattered seamounts and volcanic ridges, with a shorter history than that of Walvis, but with a similar progressive separation of the hotspot from the axis. The oldest dated sample along the St. Helena chain is 81 Ma (O'Connor and le Roex, 1992), dredged on a seamount situated at the northeastern extremity of the chain (Fig. 1). The Cameroon line, northeast of this volcano, seems to form a bathymetric extension of the St. Helena chain into the Gulf of Guinea and linking with the African continent. However, the Cameroon lineament does not show any age progression (Fitton, 1987), and therefore cannot be directly linked to a hotspot origin. The origin of the St. Helena chain on the African plate is associated with the emplacement of the Brazilian seamounts on the American plate (O'Connor and le Roex, 1992). Geochemical (Schilling et al., 1985; Schilling, 1985) and seismological studies (Zhang and Tanimoto, 1992) indicate a migration of the St. Helena plume toward the spreading axis. Circe seamount (Fig. 1) has been proposed as the site of an active hotspot by Schilling et al. (1985). It is dated at 6.6 Ma, and may be part of a hotspot trail whose present-day location should be some 130 km SW of Circe seamount (O'Connor et al., 1999).

2.2. Age evolution

The distribution of the available volcanic ages (Fig. 1) shows a large scatter, with many volcanic edifices located in the same area displaying differences in age of more than 10 Ma. For example, at 34°S, we observe a 44.6 Ma volcanic age between sites dated at 64.4 Ma (south) and 61.6 Ma (north). This age scattering can be explained by diffuse volcanism, due either to a broad plume (several hundreds of km in diameter) or the presence of a cluster of plumes (O'Connor and Duncan, 1990). Independent geophysical data support the latter hypothesis, since numerous small-wavelength elongated features appear in filtered geoid and topography maps (Fleitout et al., 1989), which could indicate the presence of multiple narrow plumes. The likely presence of additional hotspot chains in nearby areas, such as the Circe seamount and proposed associated trail, is consistent with the probable presence of several hotspots (O'Connor et al., 1999; Schilling et al., 1985).

Some features uncorrelated with the Walvis and St. Helena plumes have also been reported, as Vema (18 Ma) and 7 East (91 Ma) seamounts south of the Walvis chain. Haxel and Dziak (2005) have detected volcano-acoustic signals around a seamount situated on the northern edge of the Walvis track at 5.22°W 32.96°S (see Fig. 1). These signals are interpreted as volcano-genic explosions suggesting present-day magmatic activity. The authors support the hypothesis that this phenomenon is not directly related to the Walvis mantle plume, but rather to extensional fracture zones along inactive segments of the chain.

The Walvis and St. Helena chains may have recorded the decrease in velocity of the African plate, that occurred between 19 and 30 Ma (O'Connor et al., 1999). According to O'Connor et al. (1999), the migration rate along the St. Helena chain changed from 30 mm/yr to 20 mm/yr at 19 Ma. This change occurred at 30 Ma along the Walvis chain, with a reduction from 31 mm/yr to 22 mm/yr. However, the plate velocity diminution has been computed considering that the chain follows a continuous NW direction (O'Connor et al., 1999), without taking into account hotspot tracks deduced from the rotation poles. Moreover, the slowdown is estimated solely on the two younger ages available for each chain, and is therefore poorly constrained.

3. Data analysis

We first compute the depth anomaly throughout the study area. Using the global age grid of Müller et al. (1997) and the GDH1 thermal subsidence model of Stein and Stein (1992), we compute the thermal subsidence, which we substract from the bathymetry (Smith and Sandwell, 1997) (Fig. 1). The resulting depth anomaly is then corrected for sediment loading (see Adam et al. (2005) for computational details), to obtain the residual bathymetry. In order to test different cooling models, we have also performed the computation with the Parsons and Sclater (1977) thermal subsidence model. The results (e.g., flux vs. time estimates) are shifted relative to each other but preserve

the variations and their amplitudes (Vidal and Bonneville, 2004). Interpretation of the buoyancy and volcanic flux variations in time are therefore independent of the thermal model used, even if their absolute value remains unconstrained.

In order to separate the swell (H_S) and volcanic edifices (H_V) components from the resulting depth anomaly grid, we adapted the MiFil method developed by Adam et al. (2005). This low-pass filtering method effectively removes the topography associated with volcanic edifices from the depth anomaly, and gives the topography corresponding to the swell component H_S, as shown for the St. Helena and the Walvis chains in Figs. 2a and b, respectively. The volcanic component H_V is thus the difference between the residual bathymetry and the swell component H_S.

The H_S and H_V data can then be used to compute both the swell volume and the volume of erupted material (volcanic edifices). The swell volume corresponds to the volume between the reference depth anomaly (zero) and the swell H_S. To estimate the volume of erupted material, we consider the volcanic topography, and calculate the associated compensating root. We assume that the volcanic loading is supported by an elastic lithosphere (Watts et al., 1975) with an elastic thickness of 7 km, as deduced from the age of the crust at the time of loading. Note that the choice of this compensation (regional), rather than a local (Airy) compensation, does not have a significant influence on the final results, as the computed volcanic volumes are unchanged (Vidal and Bonneville, 2004).

We then compute the variation of the buoyancy (Q_s), inferred from swell volume variations (Sleep, 1990), and volcanic (Q_v) fluxes through time for each of the two volcanic chains in a fashion similar to that of Vidal and Bonneville (2004). We translate a rectangular box of fixed size (1000 km long across-track and 20 km wide along-track) along the main axis of the chains to compute the variation of the swell and volcanic material along this trend. We chose to approximate the main axis by the straight traces shown in Fig. 2, since the hotspot tracks calculated from rotation poles (O'Connor and
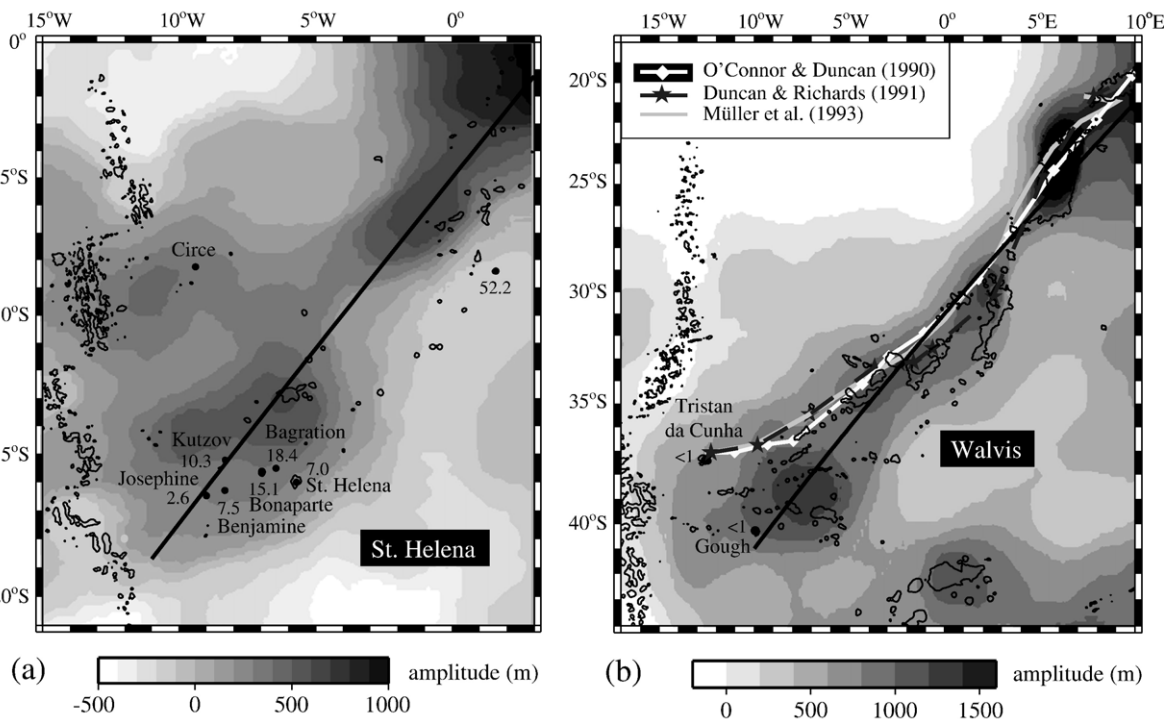

Fig. 2. Calculated swell associated with the St. Helena and Walvis chains. a) Numbers correspond to age of volcanism in million years (O'Connor and Duncan, 1990; O'Connor and le Roex, 1992). b) For readability, we only report the most recent volcanic ages (<1 Ma) along the Walvis chain. Hotspot tracks deduced from rotation poles (O'Connor and Duncan, 1990; Duncan and Richards, 1991; Müller et al., 1993) are also reported for comparison (see text). In both maps, the 2500 m isobath (thin black line) marks the position of the ridge and volcanic islands, and the bold black line indicates the traces used to study the temporal evolution of buoyancy and volcanic fluxes along both chains. The filter parameters to obtain the swell map are $r=45$ km and $R=350$ km for the minimization and filtering (see Adam et al., 2005 for details).

Duncan, 1990; Duncan and Richards, 1991; Müller et al., 1993) do not match either the swell or the volcanic chain trends. The length of the computing box, in the direction transverse to the trend, is taken large enough (1000 km) to include all the topographic features created by the hotspot and/or all its volcanic root. Therefore, volume calculations are scarcely affected by using other paths (e.g. theoretical hotspot track) for our computation instead of the straight line presented here (Vidal and Bonneville, 2004).

We also introduce the buoyancy flux (B) temporal evolution along the main axis trends. The buoyancy flux is commonly used to quantify the rate of swell formation (Sleep, 1990):

$$B = (\rho_{\mathrm{m}} - \rho_{\mathrm{w}})AV_{\mathrm{p}} \qquad (1)$$

where ρ_{m} and ρ_{w} are mantle and seawater densities respectively, A is the area of the swell in a vertical plane transverse to the hotspot track, and V_{p} the plate velocity in the hotspot frame. B can therefore be written as $B = (\rho_{\mathrm{m}} - \rho_{\mathrm{w}})Q_{\mathrm{s}}$.

4. Results

We identify swells associated with both the St. Helena and Walvis chains, and an additional one associated with the Circe seamount (Fig. 2), north of St. Helena's trail.

4.1. St. Helena swell

The St. Helena swell is composed of two circular highs, one centered at longitude 6.5°W, the other at longitude 9°W (Fig. 2a). This observation suggests that two plumes may be at the origin of the St. Helena chain. It is also interesting to note that the dated volcanoes are located slightly south of these maxima, indicating a probable influence of weakness zones of the lithosphere. The strong increase in swell amplitude, northeast of the chain (>50 Ma), will not be discussed further here, since its origin is not related to a plume, but more probably to continental processes (see Section 2.1).

4.2. Circe swell

The swell has a maximum ∼400 m amplitude and a 300–400 km width (Fig. 2a). The swell maximum is located 150 km SW of the 6.6 Ma Circe seamount, which is part of an independent hotspot trail, as suggested by O'Connor et al. (1999).

4.3. Walvis swell

The Walvis chain shows several maxima along its track. The high associated with the presumed present-day hotspot location has an amplitude of ∼1400 m and a diameter >500 km, with a maximum located NE of Gough Island and ESE of Tristan da Cunha (Fig. 2b). The dated volcanoes are here again located on the edge of the swell and not on its maximum. The middle section of the track, between 28°S and 37°S, shows two adjacent swells, with a somewhat smaller amplitude of ∼1200 m, and a width of ∼400 km. The easternmost swell is elongated along a SW–NE direction, whereas the western one has a trend close to the NS direction. Note that both trends are parallel to the volcanic chain.

Important swell amplitudes are found in the NE part of both St. Helena and Walvis chains (Fig. 2). Considering the ages of the volcanism associated with this part of the chains, these older swells (>50 Ma for St. Helena and >65 Ma for Walvis) have a too important amplitude to be considered as the result of the plume expression in an intraplate setting (see Section 2.1). Indeed, after the plume reheating, the lithosphere cools and subsides, and the subsequent mean swell amplitude should decrease. Fig. 2 shows that the swell in the older part of both chains does not follow this tendency, thus indicating that other physical processes are at stake. Therefore, the parameters we used to characterize the Walvis and St. Helena hotspot swells are not adequate to characterize the NE depth anomaly, which implies different phenomena, maybe of continental origin, occurring at different spatial scales (Van der Linden, 1980). Hence, these parts of the swells (>50 Ma for St. Helena and >65 Ma for Walvis) will not be further studied.

The hotspot tracks, deduced from rotation poles (displayed in Fig. 2b), match only the overall alignment and orientation of the swells along the central and northeasternmost portions of the chain, but are not consistent with the location of the swell at the south-westernmost end of the chain (Fig. 2b). Indeed, all the models assume that the present-day location of the plume corresponds to Tristan da Cunha, whereas the swell morphology clearly indicates that Gough is the most probable origin. Note that the shift between the plume head emplacement and the swell maximum is a classical feature of a hotspot chain. Indeed, the plume requires some time (typically, a few million years) to influence the thermal structure of the lithosphere, and hence generates a swell whose maximum is located a few hundred kilometers from the present-day plume head location, in the direction of plate motion (NE,
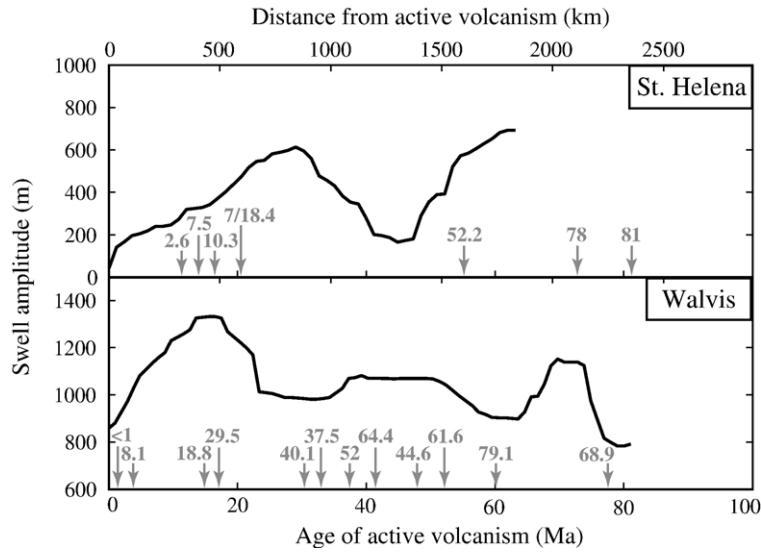
Fig. 3. Swell amplitude along the St. Helena (top) and Walvis (bottom) trends (see Fig. 1), as a function of distance from the present-day hotspot location (upper x-axis). Available ages of volcanism (gray arrows and numbers in Ma, from O'Connor and Duncan, 1990; O'Connor and le Roex, 1992) and calculated ages assuming a constant velocity (29 mm yr^{-1}) for the African plate (lower x-axis) are also shown along the horizontal axis.

here). On the other hand, hotspot volcanism is associated with the ascent of melt over the plume head, through the lithosphere and to the seafloor, and hence occurring 'upstream' from the swell maximum. Gough is therefore the best candidate for the present-day Walvis plume location. Since the tracks deduced from rotation poles do not accurately describe the plume

trajectory, we choose to describe it by the linear trends displayed in Figs. 2a and b. We assume a linear age progression of volcanism due to the drift of the African plate along them.

Fig. 3 shows the swell amplitude along the trend, as a function of distance from the zone of active volcanism. The reported ages of volcanism (O'Connor and Duncan,
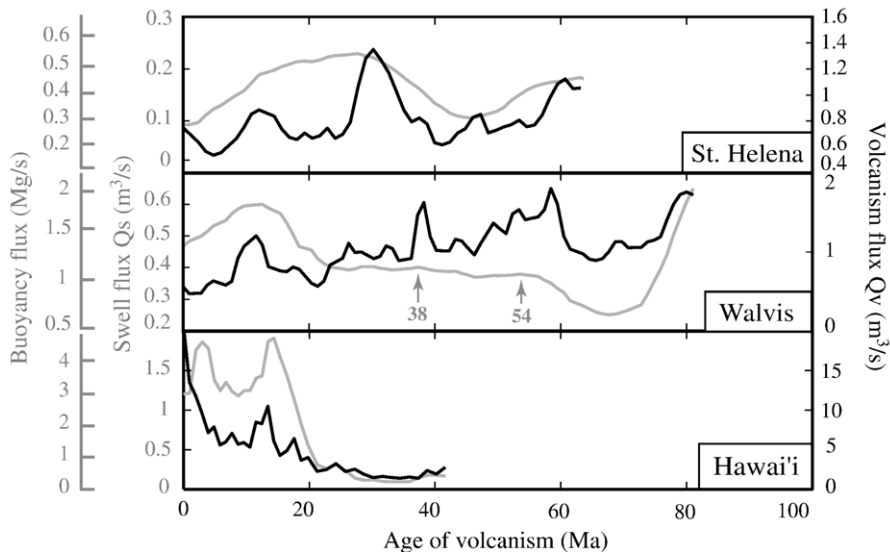

Fig. 4. Calculated buoyancy (gray) and volcanic (black) fluxes for the St. Helena (top) and Walvis (middle) chains, as a function of the interpolated age of active volcanism (see text). Gray arrows point the secondary maxima at 38 and 54 Ma in the Walvis buoyancy flux (see discussion). For comparison, the buoyancy and volcanic flux for Hawai'i are given in the bottom graph (from Vidal and Bonneville, 2004). Note the change in vertical scale, for readability.

1990; O'Connor and le Roex, 1992) show an overall age progression, but the large scatter in the data suggests that the chain formation is complex, with active volcanism extending over a large area. Distance along the proposed axes of both chains can be used as a proxy for age if we assume a constant velocity of the African plate of 29 mm yr^{-1} (O'Connor et al., 1999). O'Connor et al. (1999) also report a substantial deceleration of the African plate speed at 20–30 Ma, but this event is poorly constrained, and is not systematically observed in other plate motion models (O'Connor and Duncan, 1990; Duncan and Richards, 1991; Müller et al., 1993). We thus chose to extrapolate the volcanic ages along the trend (bottom x-axis in Figs. 3 and 4), with a constant migration rate of 29 mm yr^{-1}. We also represent in Fig. 4 the buoyancy flux B, commonly used to quantify the rate of swell formation (see Section 3).

The swell along the volcanic chains (Fig. 3) does not display the typical decay in amplitude with distance (age) from the present-day position of the hotspot. We observe instead a maximum in the swell amplitude at ∼800 km (∼30 Ma) and ∼500 km (∼15–20 Ma) along St. Helena and Walvis track, respectively. Note that the width of the swell profile along the St. Helena track is due to the presence of two swell maxima, slightly shifted off-axis (see above section, and Fig. 2a). Another large bump is observed along the Walvis chain, between 35 and 60 Ma. In the next section, we analyze the temporal variations of the deduced buoyancy fluxes.

5. Discussion

5.1. Temporal evolution of plume fluxes

5.1.1. Swell flux Q_s

The calculated buoyancy fluxes as a function of volcanic age are shown in Fig. 4. For St. Helena, we observe a single wide bump centered at ∼30 Ma, whose width can be explained by the presence of two adjacent swells (see previous section). We observe several maxima in the swell flux along the Walvis chain: a marked maximum at ∼10 Ma and two additional ones of smaller amplitude at 38 and 54 Ma. These secondary maxima are subdued in Fig. 4, due to the scaling, but they are well-visible on the Walvis swell map (Fig. 2b). The older parts of the buoyancy flux (>50 Ma for St. Helena and >65 Ma for Walvis) are not interpreted (see swell amplitude discussion, Section 4).

The Hawai'i chain, which has a shorter life span (<45 Ma) than that of the St. Helena (∼60 Ma) and Walvis chains (∼80 Ma), is probably the best characterized hotspot trail (Vidal and Bonneville, 2004), and

can be used as a reference in our study. Note that we ignore here the Emperor part, where no swell is reported, and whose volcanic flux is much smaller (Vidal and Bonneville, 2004). Hawai'i shows two important peaks at 3 and 15 Ma. It is important to note that the 3 Ma peak may not be a "real" one since plumes require some time (typically a few million years) to influence the thermal structure of the lithosphere. The swell may then not be totally formed yet at the youngest extremity. Therefore, the age difference between the two peaks in the Hawaiian swell (Fig. 4, bottom) could still increase in the next few million years.

5.1.2. Volcanic flux Q_v

The St. Helena chain displays a peak at 10 Ma, preceded by another peak at 30 Ma, in the magma production rate Q_v. Based on both the lack of correlation between variations in Q_v and Q_s (Fig. 4), and on the presence of two marked swells (Fig. 2a), we propose that the St. Helena trail is formed by two hotspots, instead of a single one. Recent evidence of the existence of two plumes beneath the younger part of St. Helena chain, given by tomography (Montelli et al., 2006), favors this hypothesis.

The Walvis chain also shows a peak at 10 Ma in the magma production rate Q_v, correlated with the main peak in the buoyancy flux profile (Fig. 4). This main peak is preceded by two secondary peaks in Q_v, at 39 and 59 Ma, also correlated with two smaller peaks in Q_s at 38 and 54 Ma (Fig. 4 and above discussion on Q_s). This correlation between Q_v and Q_s strongly suggests a common origin for both fluxes, with a single plume that peaked in activity at 10 Ma with pulsations 10–20 Ma apart. These pulsations are superimposed on an apparent long-term waning of the plume. We see indeed a progressive overall decrease in Q_v since a maximum at about 60 Ma. This decrease in the volcanic activity is also apparent in the progressive diminution of the size and density of seamounts at the seafloor (Fig. 1). In comparison, the production of magma increases drastically during the last 30 Ma for Hawai'i (Fig. 4). A peak is observed at 15 Ma along this chain with a pronounced increase to the present time, suggesting that the plume is waxing and may have not reached yet its maximal activity.

Both St. Helena and Walvis show short-term variations in magma production rate Q_v, with a periodicity of about 5 m.y., which has also been reported for Hawai'i (Vidal and Bonneville, 2004).

5.1.3. Evolution of fluxes

The most significant result of this study is that the Walvis plume does not appear to be steady state, but

rather shows pulsations at 10–20 m.y. This periodicity cannot be determined for St. Helena, as it is likely the result of the activity of two plumes and their temporal variations. A possible explanation for these pulsations is the tilt of the plume conduit due to large-scale mantle advection (Steinberger, 2000;Whitehead, 1982), as they may develop oscillations if their dip is larger than 60° (Whitehead, 1982). This mechanism has been also invoked to explain the scatter in volcanic ages along other hotspot chains such as Louisville (Koppers et al., 2004). In this study, we suggest that the observed periodicity of 10–20 m.y. may be the first estimate of the frequency of these oscillations, deduced from observed data.

Walvis also shows a marked decrease in volcanic flux Q_v through time which may reflect a progressive and steady waning of the plume and its associated activity during the last 60 Ma or more; its extinction could occur in 30 Ma if this decline continues at a similar rate. The Walvis plume conduit is not imaged by tomography models (Montelli et al., 2004; O'Neill et al., 2005), which may be also an indicator of its weakening and possible extinction. Alternatively, there is a progressive increase of the age of the lithosphere over which the volcanism is emplaced due to the migration of the ridge away from the hotspot. The resulting thickening of the lithosphere with time could play a role in this reduction of Q_v, but this interpretation is not supported by the lack of such a pattern along the St. Helena chain.

The shorter-term variations with a periodicity of ~5 m.y. observed in the magma production rate Q_v for St. Helena and Walvis (Fig. 4) have a too small periodicity to be associated with a plume tilting phenomenon, which can sustain tilts up to 60°, depending on the surrounding mantle viscosity (Steinberger, 2000). No evidence of the decorrelation of both the 10–20 and 5 m.y. pulsations can be affirmed. One possible explanation, however, could be the presence of solitary waves within the plume conduit (Whitehead and Helfrich, 1990). These perturbations have been invoked to explain both isotopic heterogeneities (West et al., 1987) and a similar 5–7 m.y. periodicity in volcanism (Vidal and Bonneville, 2004) along the Hawai'i chain (Fig. 4).

5.2. Total volumes and fluxes

We have computed the cumulative volcanic and swell volumes for the St. Helena and Walvis chains, and reported the estimation of swell volume for Circe in Table 1; owing to the lack of data, we cannot provide an estimate of its volcanic flux. In Table 1 are also reported

Table 1
Total volumes and volume fluxes of volcanic material and swell for Circe, St. Helena and Walvis (this study), and Hawai'i (from Vidal and Bonneville, 2004)

	Volcanic volume ($\times 10^5$ km^3)	Swell volume ($\times 10^5$ km^3)	Volcanic flux (m^3 s^{-1})	Swell flux (m^3 s^{-1})	Buoyancy flux (Mg s^{-1})
Circe	–	0.65	–	0.09	0.22
St. Helena	11.1	2.33	0.76	0.16	0.37
Walvis	21.4	8.79	1.00	0.41	0.96
Hawai'i	61.8	10.0	4.70	0.76	1.75

Note that the total fluxes here are calculated as a mean flux along the chain.

the values found for Hawai'i (from Vidal and Bonneville, 2004). We have also calculated the mean fluxes along each chain, which we prefer over the present-day values normally reported in the literature, as they integrate the activity and strength of hotspots over their lifespan.

Hawai'i has the greatest mean volcanic and swell fluxes, thus indicating that it is the most vigorous of all the identified plumes. Walvis and St. Helena have similar volcanic fluxes but Walvis' swell flux is three times greater than that of the St. Helena system. As St. Helena results from the combination of two plumes, we can deduce that these are two small ones. The low swell flux associated with Circe suggests that it is a weak and/or small plume.

6. Conclusion

In this paper we have presented the first characterization of the swell and volcanic fluxes and their temporal evolution along the Walvis and St. Helena hotspot trails. Both hotspot trails are associated with very broad swells, with the volcanic activity slightly offset relative to the swell maxima. For Walvis, the swell maximum shows a marked offset with respect to the proposed present-day hotspot location inferred from rotation pole reconstruction (Tristan da Cunha), suggesting that the trajectory of this plume is not accurately described by these models. We propose that Gough is the most probable present-day hotspot location. We also find a modest swell associated with the Circe seamount, north of the St. Helena trail, supporting the proposed presence of a hotspot whose location is still undetermined, and an associated volcanic chain.

The Walvis hotspot appears to be the result of a single, waning plume, that shows variations in the volcanic and swell flux at a 10–20 m.y. time-scale, and additional, shorter-term variations of about 5 m.y. in the volcanic flux. In contrast, the St. Helena chain appears to be the result of

two hotspots, which precludes the interpretation of calculated volcanic and swell fluxes in terms of temporal variability of a single plume. This chain shows also a volcanic periodicity of 5 m.y., similar to that observed along the Hawai'i chain. The 10–20 m.y. periodicity may be due to the tilting of the mantle plume conduit under mantle advection, whereas the 5 m.y. variabilities could be explained by instabilities in the conduit itself.

The estimation of the mean swell and volcanic fluxes makes it possible to compare the relative strength of the South Atlantic plumes. The strongest is Walvis, followed by the two St. Helena plumes, and probably Circe. The Hawai'i plume (Pacific), which is the reference hotspot in our study, remains the most vigorous among all these plumes.

Acknowledgments

References

Adam, C., Vidal, V., Bonneville, A., 2005. MiFil: a method to characterize seafloor swells with application to the south central Pacific. Geochem. Geophys. Geosyst. 6 (1), Q01003. doi:10.1029/2004GC000814.

Courtillot, V., Davaille, A., Besse, J., Stock, J., 2003. Three distinct types of hotspots in the Earth's mantle. Ann. Rev. Earth Planet. Sci. 205, 295–308.

Crough, S., 1983. Hotspot swells. Ann. Rev. Earth Planet. Sci. 11, 165–193.

Detrick, R.S., Watts, A.B., 1979. An analysis of isostasy in the World's Oceans, 3. Aseismic Ridges. J. Geophys. Res. 84, 3637–3653.

Duncan, R.A., Richards, M.A., 1991. Hotspots, mantle plumes, flood basalts and true polar wander. Rev. Geophys. 29, 31–50.

Fitton, J.G., 1987. The Cameroon Line, West Africa: a comparison between oceanic and continental alkaline volcanism. Geol. Soc. London Spec. Publ. 30, 273–291.

Fleitout, L., Dalloubeix, C., Moriceau, C., 1989. Small-wavelength geoid and topography anomalies in the South Atlantic Ocean: a clue to new hot-spot tracks and lithospheric deformation. Geophys. Res. Lett. 16, 637–640.

Gibson, S.A., Thompson, R.N., Day, J.A., 2006. Timescales and mechanisms of plume–lithosphere interactions: ^{40}Ar/^{39}Ar geochronology and geochemistry of alkaline igneous rocks from the Paraná-Etendeka large igneous province. Earth Planet. Sci. Lett. 251, 1–17.

Goslin, J., Sibuet, J.C., 1975. Geophysical study of the easternmost Walvis Ridge, South Atlantic: deep structure. Geol. Soc. Amer. Bull. 86, 1713–1724.

Haxel, J.H., Dziak, R.P., 2005. Evidence of explosive seafloor volcanic activity from the Walvis Ridge, South Atlantic Ocean. Geophys. Res. Lett. 32, L13609. doi:10.1029/2005GL023205.

Koppers, A.A.P., Duncan, R.A., Steinberger, B., 2004. Implications of a nonlinear ^{40}Ar/^{39}Ar age progression along the Louisville seamount trail for models of fixed and moving hot spots. Geochem. Geophys. Geosyst. 5, Q06L02. doi:10.1029/2003GC000671.

Montelli, R., Nolet, G., Dahlen, F.A., Masters, G., 2006. A catalogue of deep mantle plumes: new results from finite-frequency tomography. Geochem. Geophys. Geosyst. 7, Q11007. doi:10.1029/2006GC001248.

Montelli, R., Nolet, G., Dahlen, F.A., Masters, G., Engdahl, E.R., Hung, S., 2004. Finite-frequency tomography reveals a variety of plumes in the mantle. Science 303, 338–343.

Müller, D.M., Roest, W.R., Royer, J.-Y., Gahagan, L.M., Sclater, J.G., 1997. Digital isochrons of the world's ocean floor. J. Geophys. Res. 102, 3211–3214.

Müller, R.D., Royer, J.-Y., Lawver, L.A., 1993. Revised plate motions relative to the hotspots from combined Atlantic and Indian Ocean hotspot tracks. Geology 21, 275–278.

O'Connor, J.M., Duncan, R.A., 1990. Evolution of the Walvis Ridge-Rio Grande Rise Hot Spot System: implications for African and South America Plate motions over plumes. J. Geophys. Res. 95, 17,475–17,502.

O'Connor, J.M., le Roex, A.P., 1992. South Atlantic hot spot plume systems: 1. Distribution of volcanism in time and space. Earth Planet. Sci. Lett. 113, 17,343–17,364.

O'Connor, J.M., Stoffers, P., van den Bogaard, P., McWilliams, M., 1999. First seamount age evidence for significantly slower African plate motion since 19 to 30 Ma. Earth Planet. Sci. Lett. 171, 575–589.

O'Neill, C., Müller, D., Steinberger, B., 2005. On the uncertainties in hot spot reconstructions and the significance of moving hot spot reference frames. Geochem. Geophys. Geosyst. 6, Q04003. doi:10.1029/2004GC000784.

Parsons, B., Sclater, J., 1977. An analysis of the variation of ocean floor bathymetry and heat flow with age. J. Geophys. Res. 82, 803–827.

Schilling, J.-G., 1985. Upper mantle heterogeneities and dynamics. Nature 314, 62–67.

Schilling, J.-G., Thompson, G., Kingsley, R., Humphris, S., 1985. Hotspot-migrating ridge interaction in the South Atlantic. Nature 313, 187–191.

Sleep, N., 1990. Hotspots and mantle plumes: some phenomenology. J. Geophys. Res. 95, 6715–6736.

Smith, W.H.F., Sandwell, D.T., 1997. Global sea floor topography from satellite altimetry and ship depth soundings. Science 277, 1956–1962.

Stein, C., Stein, S., 1992. A model for the global variation in oceanic depth and heat flow with lithospheric age. Nature 359, 123–129.

Steinberger, B., 2000. Plumes in a convecting mantle: models and observations for individual hotspots. J. Geophys. Res. 105, 11,127–11,152.

Van der Linden, W.J.M., 1980. Walvis Ridge, a piece of Africa? Geology 8, 417–421.

Vidal, V., Bonneville, A., 2004. Variations of the Hawaiian hot spot activity revealed by variations in the magma production rate. J. Geophys. Res. 109, B03104. doi:10.1029/2003JB002559.

Watts, A., Cochran, J., Selzer, G., 1975. Gravity anomalies and flexure of the lithosphere: a three-dimensional study of the Great Meteor Seamount, northeast Atlantic. J. Geophys. Res. 80, 1391–1399.

West, H., Gerlach, D., Leeman, W., Garcia, M., 1987. Isotopic constraints on the origin of Hawaiian lavas from the Maui Volcanic Complex, Hawaii. Nature 330, 216–219.

Whitehead, J., 1982. Instabilities of fluid conduits in a flowing Earth — are plates lubricated by the asthenosphere? Geophys. J. R. Astron. Soc. 70, 415–433.

Whitehead, J., Helfrich, K., 1990. Magma waves and diapiric dynamics. In: Ryan, M. (Ed.), Magma transport and storage. John Wiley & Sons.

Wilson, J., 1963. A possible origin of the Hawaiian Islands. Can. J. Phys. 41, 863–870.

Zhang, Y.-S., Tanimoto, T., 1992. Ridges, hotspots and their interactions as observed in seismic velocity maps. Nature 355, 45–49.